LETTERS

Single-atom-resolved fluorescence imaging of an atomic Mott insulator

Jacob F. Sherson[1]*†, Christof Weitenberg[1]*, Manuel Endres[1], Marc Cheneau[1], Immanuel Bloch[1,2] & Stefan Kuhr[1]

The reliable detection of single quantum particles has revolutionized the field of quantum optics and quantum information processing. For several years, researchers have aspired to extend such detection possibilities to larger-scale, strongly correlated quantum systems[1,2] in order to record *in situ* images of a quantum fluid in which each underlying quantum particle is detected. Here we report fluorescence imaging of strongly interacting bosonic Mott insulators in an optical lattice with single-atom and single-site resolution. From our images, we fully reconstruct the atom distribution on the lattice and identify individual excitations with high fidelity. A comparison of the radial density and variance distributions with theory provides a precise *in situ* temperature and entropy measurement from single images. We observe Mott-insulating plateaus with near-zero entropy and clearly resolve the high-entropy rings separating them, even though their width is of the order of just a single lattice site. Furthermore, we show how a Mott insulator melts with increasing temperature, owing to a proliferation of local defects. The ability to resolve individual lattice sites directly opens up new avenues for the manipulation, analysis and applications of strongly interacting quantum gases on a lattice. For example, one could introduce local perturbations or access regions of high entropy, a crucial requirement for the implementation of novel cooling schemes[3].

Ultracold atoms in optical lattices have proved to be powerful simulators for the investigation of the static quantum phases and dynamical evolutions of strongly correlated quantum many-body systems. Prominent examples include the quantum phase transition from a superfluid to a Mott insulator[4–7] and the fermionized Tonks–Girardeau gas for bosonic particles[8,9], as well as the recently realized fermionic Mott insulator[10,11]. In all these cases, the strong interactions between the particles compared to their kinetic energy generate intriguing highly correlated quantum states that are of fundamental interest in condensed matter physics and promising for practical applications in quantum information science. For many of these applications it is of crucial importance to image the correlated many-body systems with single-atom and single-site resolution. One could then, for example, probe the evolution from a Poissonian atom number distribution into highly number-squeezed Fock states on a lattice not only globally[12] but also on a local scale. Furthermore, one should be able to observe critical phenomena directly in the *in situ* density or in spin-resolved images of the particles when approaching a quantum critical point. For applications in quantum information science, it is essential to address and manipulate single atoms on individual lattice sites. A prominent example is the one-way quantum computer[13], in which local single-particle measurements and operations are carried out after a successful global entanglement operation that creates a highly correlated cluster state.

Over the past years tremendous progress has been made in the high-resolution and single-atom sensitive detection of atoms on a lattice[14–18]. However, it has only now become possible to apply these techniques to the detection of strongly correlated quantum systems, in this work and in the work of ref. 19. Here we report on *in situ* fluorescence imaging of a Mott insulator with single-atom and single-site resolution. From a single image, we reconstruct the atom distribution on the lattice and individual thermal excitations of the Mott insulator become directly visible. This allows us to observe the number squeezing and the quality of an atomic Mott insulator down to a single lattice site. Using a simple model[20,21], we characterize the average density distribution and number fluctuations of the quantum system, and use this for an *in situ* temperature measurement. We find excellent agreement with our theory, which assumes global thermal equilibrium. Furthermore, we show how the incompressible Mott phase evolves into a compressible normal phase as the temperature is increased.

Our experiments start with an almost pure two-dimensional Bose–Einstein condensate[7] (BEC) of up to a few thousand ^{87}Rb atoms, prepared in a single pancake-shaped antinode of a vertical optical standing wave (beam waist $w_0 = 75\,\mu$m) oriented along the z axis (see Fig. 1). The lattice depth was $V_z = 26(2)E_r$ (the number in parentheses denotes the 1σ uncertainty of the last digit), where $E_r = h^2/(2m\lambda^2)$ is the recoil energy, m denotes the atomic mass of ^{87}Rb and λ the lattice wavelength. Additional beams along the x and y directions were used to load the two-dimensional quantum gas into an optical lattice. All lattice beams had a wavelength of $\lambda = 1{,}064$ nm, resulting in a lattice period of 532 nm. We detected the atoms in the lattice by high-resolution fluorescence imaging through a specially designed microscope objective with a numerical aperture of NA = 0.68 and an optical resolution (full-width at half-maximum) of about 700 nm at a wavelength of 780 nm. For detection, the lattice depths along all three directions were increased to $V_{x,y,z}/k_B \approx 300\,\mu$K before an optical molasses induced fluorescence and simultaneously laser-cooled the atoms[14,18] (see Methods). In the low-density thermal clouds (inset in Fig. 1) individual atoms are directly visible above an almost indiscernible background and their positions have a discrete spacing given by our lattice period (see Supplementary Information). During the imaging, atom pairs on a lattice site are immediately lost owing to inelastic light-induced collisions[22]. We therefore detect only the particle number modulo two on each lattice site. This amounts to recording the parity of the atom number.

The two-dimensional lattice gases used in our experiments are well described by the Bose–Hubbard model, in which particles are restricted to occupy the lowest-energy band of the lattice and their kinetic energy is characterized by a tunnelling matrix element J and an on-site two-particle interaction energy U (see refs 1 and 2). For a BEC loaded into a weak lattice potential, $U/J \ll 1$, one expects a Poissonian atom number distribution on a lattice site i, because the classical coherent matter wave field of a BEC is characterized by Glauber's coherent states. Such states, with an average filling of $\bar{n}_i$

[1]Max-Planck-Institut für Quantenoptik, Hans-Kopfermann-Straße 1, D-85748 Garching, Germany. [2]Ludwig-Maximilians-Universität, Schellingstraße 4/II, D-80799 München, Germany. †Present address: Department of Physics and Astronomy, University of Aarhus, DK-8000 Aarhus C, Denmark.
*These authors contributed equally to this work.

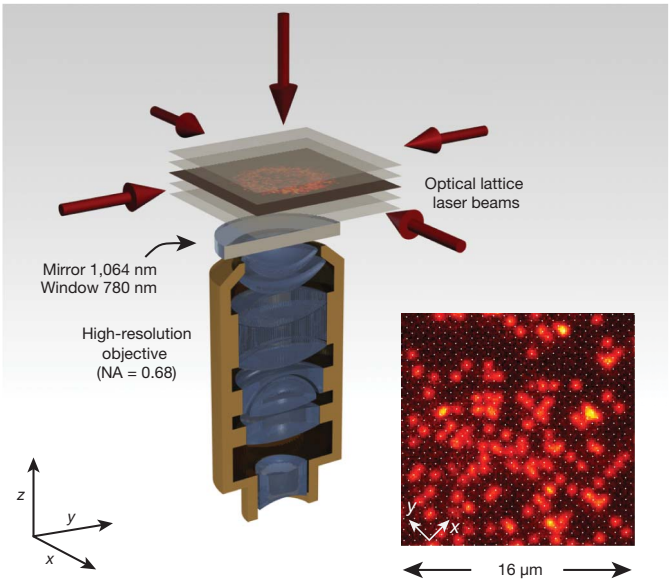

Figure 1 | Experimental set-up. Two-dimensional bosonic quantum gases are prepared in a single two-dimensional plane of an optical standing wave along the z direction, which is created by retroreflecting a laser beam ($\lambda = 1{,}064$ nm) on the coated vacuum window. Additional lattice beams along the x and y directions are used to bring the system into the strongly correlated regime of a Mott insulator. The atoms are detected using fluorescence imaging via a high-resolution microscope objective. Fluorescence of the atoms was induced by illuminating the quantum gas with an optical molasses that simultaneously laser-cools the atoms. The inset shows a section from a fluorescence picture of a dilute thermal cloud (points mark the lattice sites).

per lattice site, exhibit a corresponding variance in the particle number $\sigma_i^2 = \bar{n}_i$. When the interactions between the particles relative to their kinetic energy are increased, the system undergoes a quantum phase transition to a Mott insulating state[4–6]. For homogeneous conditions and a two-dimensional simple square lattice, this transition is expected to occur at $(U/J)_c \simeq 16.4$ (see ref. 23), where small shifts of this critical value have been reported when the system is additionally exposed to an underlying harmonic trapping potential[24]. In our case, such an additional harmonic confinement was caused by the Gaussian beam profile of our lattice beams ($1/e^2$ waist of 75 μm) and resulted in an in-plane harmonic confinement with trapping frequencies $\omega_x/(2\pi) = 72(4)$ Hz and $\omega_y/(2\pi) = 83(4)$ Hz for lattice depths of $V_{x,y} = 23(2)E_r$. For $U/J \gg (U/J)_c$ the Mott insulator can be described by neglecting the tunnelling energy of the system in the so called zero-tunnelling approximation (atomic limit). The in-trap density distribution then exhibits a pronounced shell structure of incompressible regions where the density is pinned to integer values and increases in a step-like manner from the outer wings to the inner core[5,16,25,26]. At zero temperature, the particle number variance at a lattice site is then expected to vanish ($\sigma_i^2 = 0$), resulting in perfect Fock states. For low, but still finite temperatures $k_B T \ll U$, thermal fluctuations can be induced. These fluctuations limit the quality of the number squeezing and eventually lead to a complete melting of the characteristic shell structure of a Mott insulator when the temperature is increased above the melting temperature $T_m \simeq 0.2U/k_B$ (see refs 20 and 21).

We monitored the dramatic differences in the density profiles and the on-site number fluctuations by imaging the in-trap atom distributions of a BEC and a Mott insulator in the zero-tunnelling limit for different atom numbers and temperatures (see top row of Fig. 2). For the Mott insulators, the lattices along the x and y directions were increased in S-shaped ramps within 75 ms up to values of $V_{x,y} = 23(2)E_r$. To freeze out the atom distribution of a BEC, we ramped up the lattices within 0.1 ms. Using the point spread function of our optical imaging system we were able to reconstruct the atom number distribution on the lattice with single-site and single-atom resolution via an image processing algorithm (see Methods). It works

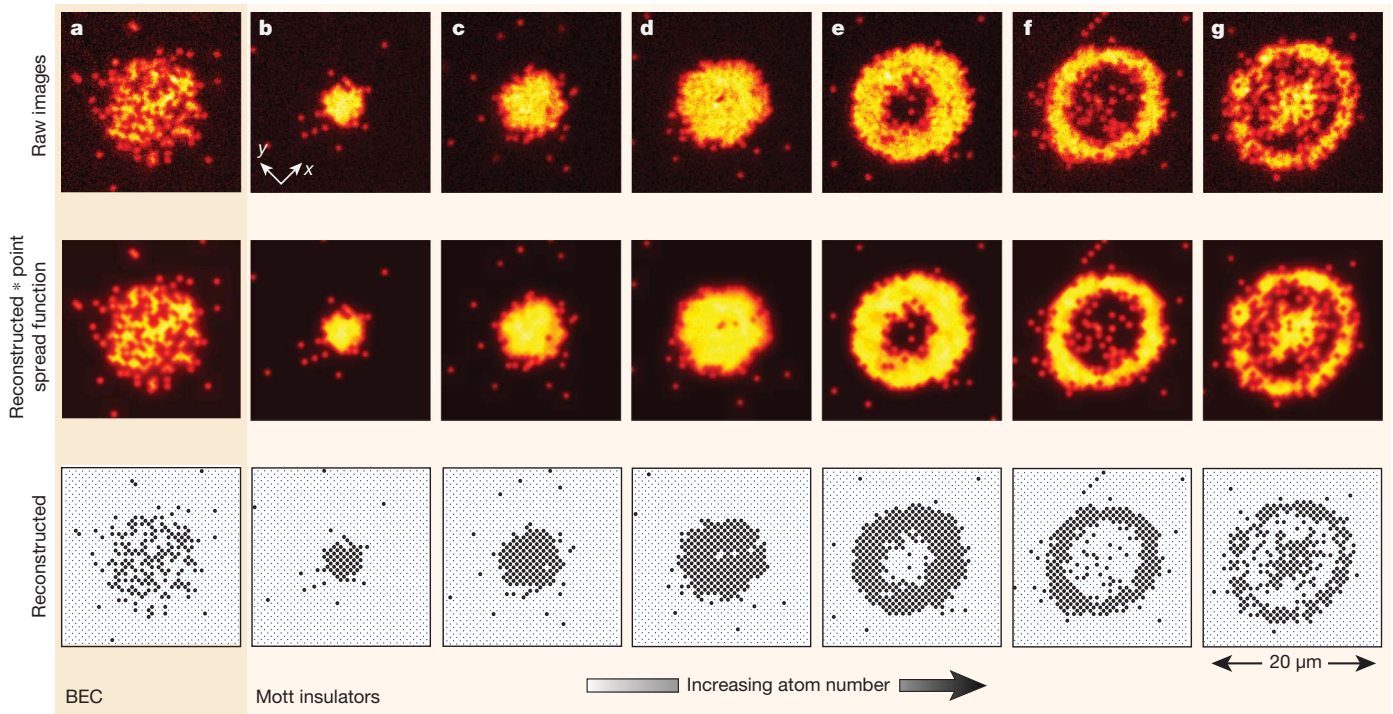

Figure 2 | High-resolution fluorescence images of a BEC and Mott insulators. The top row shows experimentally obtained raw images of a BEC (**a**) and Mott insulators for increasing particle numbers (**b**–**g**) in the zero-tunnelling limit. The middle row shows numerically reconstructed atom distribution on the lattice. The images were convoluted with the point spread function (* indicates the convolution operator) of our imaging system for comparison with the original images. The bottom row shows the reconstructed atom number distribution. Each circle indicates a single atom; the points mark the lattice sites. The BEC and Mott insulators were prepared with the same in-plane harmonic confinement (see Supplementary Information for the Bose–Hubbard model parameters of our system).

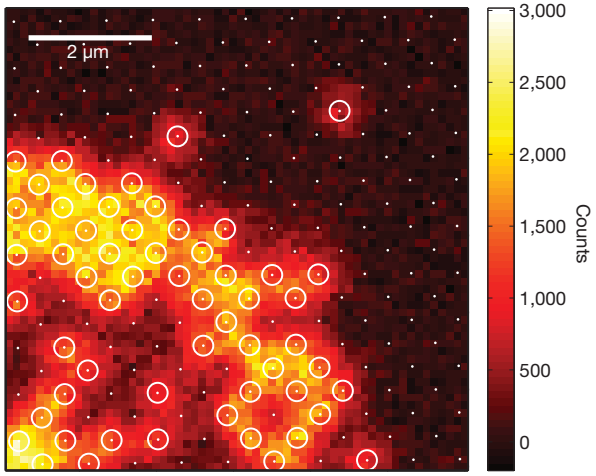

Figure 3 | Identification of single atoms in a high-resolution image. The points mark the centres of the lattice sites; circles indicate those sites where our deconvolution algorithm determined the presence of an atom. The image is a zoom into the upper right part of Fig. 2g.

reliably even in the regions of high atomic density, as illustrated in Fig. 3.

To compare the digitally reconstructed atom distribution (see bottom row of Fig. 2) with the raw images, we show the reconstructed distribution convoluted with the point spread function in the middle row of Fig. 2. For a BEC with a Poissonian atom number distribution the average filling one detects due to the parity measurement in the fluorescence imaging is $\bar{n}_{i,\mathrm{det}} = 1/2[1-\exp(-2\bar{n}_i)]$, which saturates at $\bar{n}_{i,\mathrm{det}} = 0.5$ for $\bar{n}_i \gtrsim 1.5$. In this limit, the detected atom number variance then saturates accordingly at $\sigma^2_{i,\mathrm{det}} = 0.25$. Indeed, for a BEC, we observed that the recorded atomic density exhibits large atom number fluctuations from site to site. In contrast, for a Mott insulator we obtain plateaus of constant integer density, with almost vanishing fluctuations. For increasing particle numbers, the images in Fig. 2 show how successive Mott insulator shells are formed and appear as alternating rings of one and zero atoms per site owing to our parity measurement. In both the raw images and the reconstructed ones, individual defects are directly visible. The high symmetry of our atom clouds reflects the high optical quality of our lattice potentials. A small ellipticity is caused by the different harmonic trapping frequencies ω_x and ω_y.

We used the reconstructed site occupation numbers to determine the temperature of the sample based on a single image. For deep lattices, $U/J \simeq 300$, as used in our experiments for Mott insulators, tunnelling becomes completely suppressed such that coherent particle–hole fluctuations are expected to be negligible and defects are induced only by thermal fluctuations. The symmetry of our clouds allowed us to average the data azimuthally, taking into account the ellipticity, and to obtain radial profiles for the average density $\bar{n}_{\mathrm{det}}(r)$ and variance $\sigma^2_{\mathrm{det}}(r)$ (see Fig. 4a and b and Methods). We fitted analytic expressions derived in the zero-tunnelling regime (see Methods) to our data. The results of such a fit for an $n = 1$ ($0 < \mu/U < 1$) and an $n = 2$ ($1 < \mu/U < 2$) Mott insulator are displayed in Fig. 4a and b. The Mott insulator regions can be identified as connected regions of constant integer density and vanishing on-site number fluctuations, which in the zero-tunnelling limit of the Hubbard model signify the presence of incompressible Mott domains[24]. For both density profiles and atom number variances we find excellent agreement between the experimental data and the theoretical model for all radial distances. This supports the assumption that our system is in global thermal equilibrium, in contrast to ref. 27. The extracted temperatures of $T = 0.090(5)\,U/k_{\mathrm{B}}$ and $T = 0.074(5)\,U/k_{\mathrm{B}}$ for the $n = 1$ and $n = 2$ data are well below the

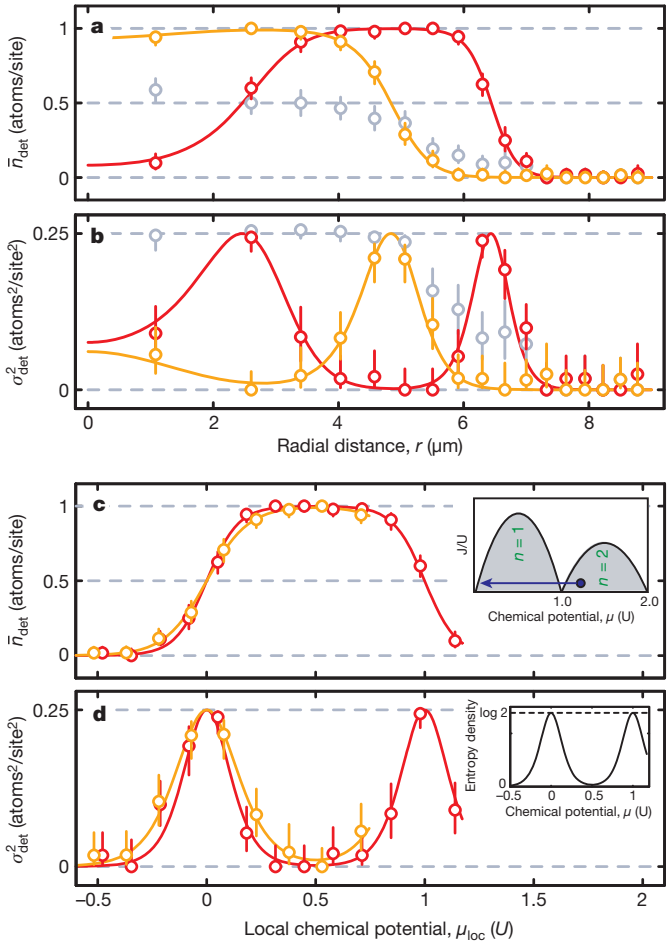

Figure 4 | Radial atom density and variance profiles. Radial profiles were obtained from the digitally reconstructed images by azimuthal averaging. **a**, **b**, Yellow and red points correspond to the $n = 1$ and $n = 2$ Mott insulator images of Fig. 2d and e. The grey points were obtained from a BEC (data from Fig. 2a) for reference. The displayed statistical error bars are Clopper–Pearson 68% confidence intervals for the binomially distributed number of excitations. For the Mott insulators, both average density $\bar{n}_{\mathrm{det}}(r)$ and variance $\sigma^2_{\mathrm{det}}(r)$ profiles are fitted simultaneously with the model functions of equations (1) and (2) (see Methods) with T, μ and $r_0^2 = 2U/(m\omega_x\omega_y)$ as free parameters. For the two curves, the fits yielded temperatures $T = 0.090(5)U/k_{\mathrm{B}}$ and $T = 0.074(5)U/k_{\mathrm{B}}$, chemical potentials $\mu = 0.73(3)U$ and $\mu = 1.17(1)U$, and radii $r_0 = 5.7(1)$ μm and $r_0 = 5.95(4)$ μm, respectively. From the fitted values of T, μ and r_0, we determined the atom numbers of the system to $N = 270(20)$ and $N = 529(8)$. **c**, **d**, The same data plotted versus the local chemical potential using the local-density approximation. The inset of **c** is a Bose–Hubbard phase diagram ($T = 0$) showing the transition between the characteristic Mott insulator lobes (grey shading) and the superfluid region. The straight line with arrow shows the part of the phase diagram existing simultaneously at different radii in the trap owing to the external harmonic confinement. The inset of **d** shows the entropy density calculated for the displayed $n = 2$ Mott insulator.

Mott insulator melting temperature T_{m}. Our temperature measurements are conservative, because all defects are attributed to thermal excitations in our model. However, defects might for example also arise from 'collateral damage' caused by atoms undergoing the light-induced collisions. For reference, we show the corresponding data obtained by freezing out the atom distribution of a BEC. We observe the expected saturation of $\bar{n}_{\mathrm{det}}$ at 0.5 together with a maximum variance of σ^2_{det} at 0.25. We note that the thermal shells surrounding a Mott insulator core also exhibit this maximum variance and can be as narrow as one to two lattice sites. In Fig. 4c and d we plot both Mott insulator data sets versus local chemical potential. In a single image, we thus mapped out an entire line in the phase diagram as illustrated in the inset of Fig. 4c. The slightly different temperatures of the two

Mott insulators are clearly visible in the different widths of the variance curves.

Our measurements also confirm with unprecedented clarity that the entropy of the strongly correlated quantum gas is concentrated around the Mott insulating regions, whereas in the centre of a Mott insulator, for local chemical potentials of $\mu_{loc} = (n + 1/2)U$, number fluctuations are completely suppressed and the entropy density is essentially zero. For the lowest observed temperature of $T = 0.074(5)\,U/k_B$ we calculate a 99.7(1)% probability of unity occupation in the centre of the $n = 1$ Mott-insulating plateau. Using the zero-tunnelling model, we can also extract the total entropy per particle for our system $S/(Nk_B) = 0.34(2)$ (see Methods) which is around the critical entropy for quantum magnetism[28].

Finally, we show how a Mott insulator melts, as the temperature (or entropy) of the quantum gas is increased (see Fig. 5). At constant total chemical potential but increasing temperatures, we observe that the Mott domains gradually vanish. Although there is no sharp transition to a normal fluid state in this case, Mott plateaus and number squeezing degrade rapidly, once $T \gtrsim T_m$ (see Fig. 5d and e), as predicted in ref. 20.

In summary, we have demonstrated single-site- and single-particle- resolved detection of a strongly correlated system in an optical lattice. Our method can be extended to investigate quantum critical phenomena, density–density correlations or even non-local string-operators that are inaccessible in condensed matter experiments. Our imaging system can be used to focus an off-resonant laser beam onto a single atom and thereby allow single-site manipulation of the atomic qubits[29]. This opens up a new avenue for experiments with ultracold quantum gases, where for example, novel cooling schemes may be applied by accessing regions of high entropy[3]. For future work it would be interesting to investigate how entropy propagates in strongly correlated systems, after injecting it on a local scale into the system. Atoms in the Mott insulator with one atom per lattice site are also very promising as a quantum register for scalable quantum computing, especially with the very low defect density shown here.

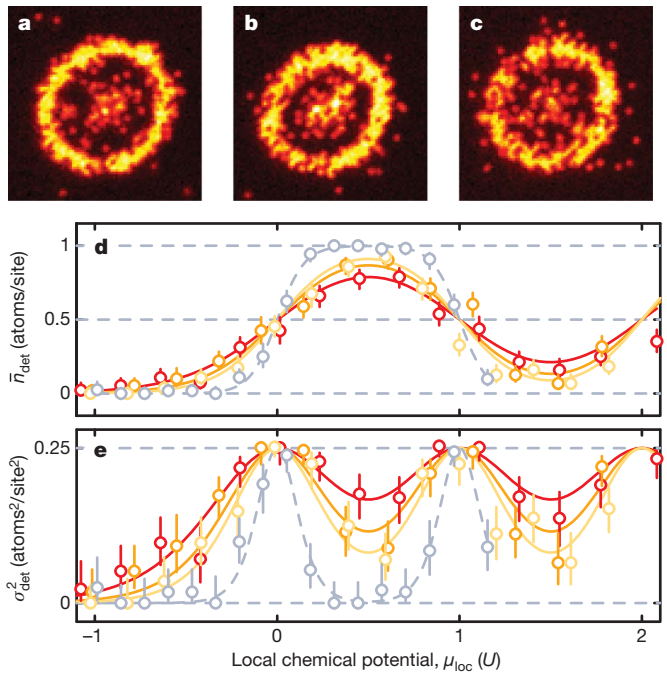

Figure 5 | Melting of a Mott insulator. a–c, Strongly correlated atomic samples for three different temperatures and constant total chemical potential in the zero-tunnelling limit. For higher temperatures, an increased number of independent particles or holes appear. The data shown was binned 2×2. **d, e**, Density and variance profiles as a function of chemical potential, determined as described in the caption of Fig. 4. Red, orange and yellow points correspond to the data sets from **a**, **b** and **c**, respectively. Grey points correspond to the low-temperature $n = 2$ Mott insulator of Fig. 2e and Fig. 4 with $T = 0.074(5)U/k_B$ and $\mu = 1.17(1)U$. The parameters extracted from the radial fits are $T = 0.17(1)U/k_B$, $\mu = 2.08(4)U/k_B$ for **a**, $T = 0.20(2)U/k_B$, $\mu = 2.10(5)U/k_B$ for **b** and $T = 0.25(2)U/k_B$, $\mu = 2.06(7)U/k_B$ for **c**.

METHODS SUMMARY

We prepared a single two-dimensional system using a position-dependent microwave transfer in a magnetic field gradient, before evaporatively cooling the atoms in the z lattice. We imaged the atoms with a microscope objective located outside the vacuum chamber. The atoms scatter fluorescence photons from an optical molasses that simultaneously laser-cools the atoms. We reconstructed the atom number distribution from the fluorescence images with a deconvolution algorithm that uses a model of the experimentally determined point spread function. The algorithm takes into account varying fluorescence levels per atom and has a fidelity of about 99.5%. An analytic model is used to calculate the radial atom number distribution and variance in the zero-tunnelling limit. Further details may be found in the online-only Methods and in the Supplementary Information.

Full Methods and any associated references are available in the online version of the paper at www.nature.com/nature.

Received 17 June; accepted 27 July 2010.
Published online 18 August 2010.

1. Jaksch, D. & Zoller, P. The cold atoms Hubbard toolbox. *Ann. Phys.* **315,** 52–79 (2005).
2. Bloch, I., Dalibard, J. & Zwerger, W. Many-body physics with ultracold gases. *Rev. Mod. Phys.* **80,** 885–964 (2008).
3. Bernier, J.-S. *et al.* Cooling fermionic atoms in optical lattices by shaping the confinement. *Phys. Rev. A* **79,** 061601(R) (2009).
4. Fisher, M. P. A., Weichman, P. B., Grinstein, G. & Fisher, D. S. Boson localization and the superfluid-insulator transition. *Phys. Rev. B* **40,** 546–570 (1989).
5. Jaksch, D., Bruder, C., Cirac, J. I., Gardiner, C. & Zoller, P. Cold bosonic atoms in optical lattices. *Phys. Rev. Lett.* **81,** 3108–3111 (1998).
6. Greiner, M., Mandel, M., Esslinger, T., Hänsch, T. & Bloch, I. Quantum phase transition from a superfluid to a Mott insulator in a gas of ultracold atoms. *Nature* **415,** 39–44 (2002).
7. Spielman, I. B., Phillips, W. D. & Porto, J. V. Mott-insulator transition in a two-dimensional atomic Bose gas. *Phys. Rev. Lett.* **98,** 080404 (2007).
8. Paredes, B. *et al.* Tonks-Girardeau gas of ultracold atoms in an optical lattice. *Nature* **429,** 277–281 (2004).
9. Kinoshita, T., Wenger, T. & Weiss, D. S. Observation of a one-dimensional Tonks-Girardeau gas. *Science* **305,** 1125–1128 (2004).
10. Jördens, R., Strohmaier, N., Günter, K., Moritz, H. & Esslinger, T. A Mott insulator of fermionic atoms in an optical lattice. *Nature* **455,** 204–207 (2008).
11. Schneider, U. *et al.* Metallic and insulating phases of repulsively interacting fermions in a 3D optical lattice. *Science* **322,** 1520–1525 (2008).
12. Gerbier, F., Fölling, S., Widera, A., Mandel, O. & Bloch, I. Probing number squeezing of ultracold atoms across the superfluid-Mott insulator transition. *Phys. Rev. Lett.* **96,** 090401 (2006).
13. Raussendorf, R. & Briegel, H. J. A. One-way quantum computer. *Phys. Rev. Lett.* **86,** 5188–5191 (2001).
14. Nelson, K. D., Li, X. & Weiss, D. S. Imaging single atoms in a three-dimensional array. *Nature Phys.* **3,** 556–560 (2007).
15. Gericke, T., Würtz, P., Reitz, D., Langen, T. & Ott, H. High-resolution scanning electron microscopy of an ultracold quantum gas. *Nature Phys.* **4,** 949–953 (2008).
16. Gemelke, N., Zhang, X., Hung, C.-L. & Chin, C. *In situ* observation of incompressible Mott-insulating domains in ultracold atomic gases. *Nature* **460,** 995–998 (2009).
17. Karski, M. *et al.* Nearest-neighbor detection of atoms in a 1D optical lattice by fluorescence imaging. *Phys. Rev. Lett.* **102,** 053001 (2009).
18. Bakr, W. S., Gillen, J. I., Peng, A., Fölling, S. & Greiner, M. A quantum gas microscope for detecting single atoms in a Hubbard-regime optical lattice. *Nature* **462,** 74–77 (2009).
19. Bakr, W. S. *et al.* Probing the superfluid-to-Mott insulator-transition at the single-atom level. *Science* 329 547–550 (2010).
20. Gerbier, F. Boson Mott insulators at finite temperatures. *Phys. Rev. Lett.* **99,** 120405 (2007).
21. Ho, T.-L. & Zhou, Q. Intrinsic heating and cooling in adiabatic processes for bosons in optical lattices. *Phys. Rev. Lett.* **99,** 120404 (2007).
22. DePue, M. T., McCormick, C., Winoto, S. L., Oliver, S. & Weiss, D. S. Unity occupation of sites in a 3D optical lattice. *Phys. Rev. Lett.* **82,** 2262–2265 (1999).
23. Krauth, W. & Trivedi, N. Mott and superfluid transitions in a strongly interacting lattice boson system. *Europhys. Lett.* **14,** 627–632 (1991).
24. Rigol, M., Batrouni, G. G., Rousseau, V. G. & Scalettar, R. T. State diagrams for harmonically trapped bosons in optical lattices. *Phys. Rev. A* **79,** 053605 (2009).
25. Fölling, S., Widera, A., Müller, T., Gerbier, F. & Bloch, I. Formation of spatial shell structure in the superfluid to Mott insulator transition. *Phys. Rev. Lett.* **97,** 060403 (2006).

26. Campbell, G. K. *et al.* Imaging the Mott insulator shells by using atomic clock shifts. *Science* **313,** 649–652 (2006).
27. Hung, C.-L., Zhang, X., Gemelke, N. & Chin, C. Slow mass transport and statistical evolution of an atomic gas across the superfluid-Mott-insulator transition. *Phys. Rev. Lett.* **104,** 160403 (2010).
28. Capogrosso-Sansone, B., Söyler, S. G., Prokof'ev, N. V. & Svistunov, B. V. Critical entropies for magnetic ordering in bosonic mixtures on a lattice. *Phys. Rev. A* **81,** 053622 (2010).
29. Zhang, C., Rolston, S. L. & Das Sarma, S. Manipulation of single neutral atoms in optical lattices. *Phys. Rev. A* **74,** 042316 (2006).

Supplementary Information is linked to the online version of the paper at www.nature.com/nature.

Acknowledgements We thank R. Glöckner and R. Labouvie for assistance during the set-up of the experiment and S. Trotzky for discussions. We acknowledge funding by the MPG, the DFG, the Stiftung Rheinland-Pfalz für Innovation, the Carl-Zeiss Stiftung, the EU (NAMEQUAM, AQUTE and Marie Curie fellowships to J.F.S. and M.C.).

Author Contributions All authors contributed to the construction of the apparatus, acquisition and analysis of the data, and the writing of this manuscript.

Author Information Reprints and permissions information is available at www.nature.com/reprints. The authors declare no competing financial interests. Readers are welcome to comment on the online version of this article at www.nature.com/nature. Correspondence and requests for materials should be addressed to S.K. (stefan.kuhr@mpq.mpg.de).

METHODS

Preparation of a single two-dimensional system. We started by loading atoms from a magnetic quadrupole trap into a single beam optical dipole trap (1,064 nm, beam waist $w_0 = 40\,\mu m$). By translating the focus of the dipole trap using mirrors on a motorized micrometre stage, the atoms were transported in front of the high-resolution imaging system within 2.5 s. A magnetic quadrupole field the centre of which was shifted below the trap compressed the cloud in the axial direction of the dipole trap laser beam. After 500 ms of evaporative cooling in this hybrid trap configuration, we transferred the atoms into the z lattice. It is oriented along the optical axis of the imaging system, parallel to gravity, and superimposed with the hybrid trap. Initially we populated 60 antinodes (slices) of the standing wave, creating independent two-dimensional systems. To extract a single two-dimensional system, we used position-dependent microwave transfer in a magnetic field gradient. The gradient of $\partial B/\partial z = 24\,G\,cm^{-1}$ (together with a bias field of 32 G) was produced with a single coil placed 50 mm above the atoms; the coil axis coincides with the z lattice beam. Our magnetic field gradient results in a position-dependent frequency shift $\partial\nu/\partial z \approx 5\,kHz\,\mu m^{-1}$ of the $|F = 1, m_F = -1\rangle \leftrightarrow |F = 2, m_F = -2\rangle$ transition. An initial microwave frequency sweep over 1 MHz brought all atoms from $|F = 1, m_F = -1\rangle$ to $|F = 2, m_F = -2\rangle$. We then transferred atoms from one slice back to the $|F = 1, m_F = -1\rangle$ state using a resonant Blackman pulse of 5 ms duration. All atoms remaining in $F = 2$ were removed from the trap by a laser pulse resonant with the $F = 2 \rightarrow F' = 3$ transition. We then evaporatively cooled the atoms by ramping down the intensity of the z lattice from $300E_r$ to $\sim 25E_r$ within 1.5 s, while simultaneously tilting the potential along the horizontal direction with a magnetic field gradient[30]. Depending on the end point of this evaporation, we created BECs with atom numbers ranging from 50 to 2,000.

Imaging single atoms in the lattice. Our microscope objective was custom made (Leica Microsystems) and is located outside the vacuum chamber with a working distance of 13 mm. We detected the atoms by illuminating them with an optical molasses, red detuned with respect to the free space resonance by 45 MHz. It consists of two pairs of retroreflected laser beams superimposed with the horizontal lattice axes. A third z-molasses laser beam aligned in reverse direction through the imaging system provided cooling in the vertical direction. The total scattering rate from all laser beams was $\sim$60 kHz. With our total detection efficiency of $\sim$9% (solid angle 15%, transmission of all optical elements 71%, camera quantum efficiency 85%), we collect about 5,000 photons per atom within our illumination time of 900 ms. To ensure a homogeneous illumination of all atoms, we scanned the retro-reflecting mirrors of the horizontal molasses beams (at frequencies of 300 Hz and 400 Hz) using piezo elements and mutually detuned the molasses beams by 43 Hz. Additionally, we spatially scanned the z-molasses beam across the cloud at a frequency of 100 Hz and an amplitude of 35 μm. We also corrected for an interference effect (etaloning) of the charge-coupled device (CCD) camera, which caused a spatially dependent signal strength. We carefully optimized the molasses parameters to minimize hopping of the atoms to adjacent lattice sites, by taking two consecutive images of the same cloud for the first 400 ms and the last 400 ms of our 900-ms illumination period. From the analysis of several of these double images, we found that about 0.5% of the atoms hop during the molasses illumination. Before switching on the molasses, we removed the atoms in the doubly occupied sites with a 50-ms pulse on the $F = 2$ to $F' = 3$ transition, which is 6.8 GHz red detuned for the atoms in $F = 1$, but efficiently excites into the molecular potentials.

For the horizontal optical lattice laser beams we used two single-mode fibre amplifiers seeded with the same narrowband solid-state laser, whereas the vertical lattice beam was derived from an independent solid-state laser. The horizontal axes were mutually detuned by 220 MHz and had orthogonal polarizations. We obtained about 10 W per lattice axis at the experiment, yielding trap depths of about 300 μK.

Reconstruction of the atom number distribution. We developed a deconvolution algorithm to reconstruct the atom number distribution from a fluorescence image. It uses a model of the point spread function of our imaging system that was determined from averaging over many images of isolated individual atoms (see Supplementary Information). The algorithm tries different model-configurations for each lattice site and its nearest neighbours in order to minimize the difference of the original image with the reconstructed one. This reconstructed image was obtained by convoluting the atom number distribution with our point spread function (see middle row of Fig. 2). The algorithm allows for a variance of the fluorescence level of each atom within ±20% of the mean photon counts. These varying fluorescence levels arise partially from the inhomogeneous intensity of the molasses light. We additionally found an increase in the fluorescence level of about 10–20% in the centre of very dense $n = 1$ shells of a Mott insulator, compared with the isolated atoms in the outer part of the images. This effect might arise from the partial coherence of the light scattered by the atoms, combined with their regular distribution in the lattice.

We have evaluated the fidelity of the reconstruction algorithm by creating simulated images of a known atom distribution using the point spread function of our imaging system, the Poissonian and super-Poissonian noise contributions of the light hitting the electron-multiplying CCD camera (including the amplification process), and the site-to-site fluorescence fluctuations of ±20%. Running the reconstruction algorithm over several hundred of such randomly generated images of Mott insulators at finite temperatures, we find a reconstruction fidelity of $\sim$99.5%. In our experiment, the main limitations of the fidelity are atom losses during the detection process due to collisions with background gas atoms. We measured that about 1% of the atoms are lost during the 900-ms detection period, which corresponds to a trap lifetime of $\sim$75 s.

Radial atom number distribution and variance. In the zero-tunnelling regime (the 'atomic limit' of a Mott insulator), the atom number distribution at a lattice site at radius r is given by $P_r(n) = e^{\beta[\mu_{loc}(r)n - E_n]} \Big/ Z(r)$, where $Z(r) = \sum_n e^{\beta[\mu_{loc}(r)n - E_n]}$ is the grand canonical partition function, $\beta = 1/(k_B T)$, $\mu_{loc}(r)$ is the local chemical potential and $E_n = Un(n-1)/2$ is the interaction energy. Using a local density approximation, we define μ_{loc} in terms of the global chemical potential μ and the external harmonic trapping confinement: $\mu_{loc}(r) = \mu - 0.5m\left(\omega_x^2 x^2 + \omega_y^2 y^2\right)$. Taking the light-induced losses into account, we calculate the expected detected density at different radii:

$$\bar{n}_{det}(r) = \frac{1}{Z(r)} \sum_n \mathrm{mod}_2(n)\, e^{\beta[\mu_{loc}(r)n - E_n]} \quad (1)$$

In the presence of light-induced collisions $\overline{n_{det}^2}(r) = \bar{n}_{det}(r)$ and the detected variance is therefore simply:

$$\sigma_{det}^2(r) = \bar{n}_{det}(r) - \bar{n}_{det}^2(r) \quad (2)$$

We extracted radial density and variance profiles from the reconstructed two-dimensional atom distribution of a single image. For this, we first determined the centre of the cloud, and then binned the lattice sites according to their distance from the centre, thereby correcting for the ellipticity of 10%. The bin sizes were chosen to be larger near the centre to have sufficient statistics.

We fitted the experimental profiles to equations (1) and (2) and extracted the temperature and the global chemical potential. These can then be used to calculate the original occupation number probability $P_r(n)$. Inserting the radius corresponding to $\mu_{loc} = 0.5\ U$ we extract the maximal theoretical unity occupation probability. We can furthermore calculate the local entropy density $S_{loc}(r) = -k_B \Sigma_n P_r(n) \ln[P_r(n)]$. Summing the density and entropy density over the lattice sites we calculate the total number of particles $N = 529(8)$ and the total entropy $S/k_B = 180(12)$ given the fitted values of T and μ from the $n = 2$ data of Fig. 4. This gives the entropy per particle $S/(Nk_B) = 0.34(2)$.

30. Hung, C.-L., Zhang, X., Gemelke, N. & Chin, C. Accelerating evaporative cooling of atoms into Bose-Einstein condensation in optical traps. *Phys. Rev. A* **78**, 011604 (2008).